Magnetic resonance in nanoparticles: between ferro- and paramagnetism

2007 J. Phys.: Condens. Matter 19 246208

(http://iopscience.iop.org/0953-8984/19/24/246208)

IOP PUBLISHING JOURNAL OF PHYSICS: CONDENSED MATTER

J. Phys.: Condens. Matter **19** (2007) 246208 (15pp) doi:10.1088/0953-8984/19/24/246208

Magnetic resonance in nanoparticles: between ferro- and paramagnetism

N Noginova[1], F Chen[1], T Weaver[1], E P Giannelis[2], A B Bourlinos[3] and V A Atsarkin[4]

[1] Norfolk State University Center for Materials Research, Norfolk, VA, USA
[2] Cornell University, Ithaca, NY, USA
[3] Institute of Materials Science, NCSR Demokritos, Athens, Greece
[4] Institute of Radio Engineering and Electronics RAS, Moscow, Russia

Received 6 November 2006, in final form 30 April 2007
Published 22 May 2007
Online at stacks.iop.org/JPhysCM/19/246208

Abstract

Magnetic nanoparticles of γ-Fe_2O_3 coated with organic molecules and suspended in liquid and solid matrices, as well as non-diluted magnetic fluid, have been studied by electron magnetic resonance (EMR) at 77–380 K. Slightly asymmetric spectra observed at room temperature become much broader and symmetric, and shift to lower fields upon cooling. An additional narrow spectral component (with a line-width of 30 G) is found in diluted samples; its magnitude obeys the Arrhenius law with an activation temperature of about 850 K. The longitudinal spin-relaxation time, $T_1 \approx 10$ ns, is determined by a specially developed modulation method. The angular dependence of the EMR signal position in field-freezing samples points to substantial alignment, suggesting the formation of dipolar-coupled aggregates.

The shift and broadening of the spectrum upon cooling are assigned to the effect of the surface-related anisotropy. To describe the overall spectral shape, the 'quantization' model is used which includes summation of resonance transitions over the whole energy spectrum of a nanoparticle considered as a giant exchange cluster. This approach, supplemented with some phenomenological assumptions, provides satisfactory agreement with the experimental data.

(Some figures in this article are in colour only in the electronic version)

1. Introduction

Magnetic nanoparticles have attracted considerable interest due to their unusual magnetic properties and are promising for many technological applications in nanoscale engineering, catalysis, mineralogy, biology and medicine (for a review, see [1, 2]). There is also a very important and interesting fundamental issue: nanometre-scale magnetic objects are at the interface between quantum dynamics of several interacting spins and many-particle behaviour

commonly described in terms of classical thermodynamics. The gap between dynamic (reversible) and thermodynamic (irreversible) approaches represents one of the most general problems in physics. Thus, by studying magnetic nanoparticles one can obtain essential information on this intriguing problem.

Among the many publications on magnetic nanoparticles, there are a considerable number of studies performed using electron magnetic resonance (EMR) methods. The theory of magnetic resonance in superparamagnetic systems was developed in [3–5], based on the classical equation of motion for a magnetic moment $\boldsymbol{\mu}$ under conditions of ferromagnetic resonance (FMR). The main result obtained in this theory is a kind of averaging caused by thermal reorientations of the magnetic moment, leading to the effective reduction of the anisotropy field with increased temperature.

A number of magnetic resonance experiments have been performed by various authors on assemblies of randomly oriented nanoparticles (as a rule, nanoparticles were embedded in a diamagnetic matrix to weaken or even exclude the inter-particle interaction) [6–19]. The agreement between experimental data and theoretical predictions is, however, rather poor and does not provide an opportunity for accurate quantitative analysis of the experimental results. The only exception is the high-temperature limit where, according to the theory, the spectrum progressively collapses into a single nearly Lorentzian line. At lower temperatures, the specific pattern predicted by the theory was not observed; instead, significant broadening of the single line was found together with its progressive shifting to lower fields with cooling.

Thus, further studies and interpretation of the EMR data in ensembles of magnetic nanoparticles remain very important. Such an investigation, supported by a theoretical approach combining ferromagnetic (classical) and paramagnetic (quantum) considerations, is the main purpose of this work.

2. Experimental techniques and results

The experimental samples were prepared using a solvent-free ferrofluid containing surface functionalized maghemite (γ-Fe_2O_3) nanoparticles. Such a ferrofluid was produced by attaching a corona of flexible chains onto maghemite nanoparticles. Specifically, reaction of a positively charged organosilane ($(CH_3O)_3Si(CH_2)_3N^+(CH_3)(C_{10}H_{21})_2Cl^-$) with surface hydroxyl groups on the nanoparticles leads to a permanent covalent attachment to the surface and renders the nanoparticles positively charged. A counter anion is present to balance the charge leading to a hybrid nanoparticle salt. The sulfonate anions ($R(OCH_2CH_2)_7O(CH_2)_3SO_3^-$, R: C_{13}–C_{15} alkyl chain) were used, yielding a liquid at room temperature with a nanoparticle content of around 40 wt% [20]. A TEM picture and the schematic of the nanoparticles are shown in figure 1.

The size distribution of the nanoparticles was found to be nearly log-normal, with a mean diameter of 4.8 nm and dispersion $\sigma = 0.15$. Apart from well-separated nanoparticles, large clusters (aggregates) are also seen in the TEM picture. To prepare experimental samples with different concentrations, the nanoparticles were dispersed in liquid (toluene) and solid (polystyrene) matrices.

The electron magnetic resonance studies were performed using a EMX Bruker electron paramagnetic resonance (EPR) spectrometer operating at 9.8 GHz (X band); the modulation frequency was 100 kHz. A commercial gas-flow cryostat was used to vary the temperature of the sample in the range of 77–360 K inside the quartz Dewar tube in the microwave cavity. The cavity itself was kept at room temperature, and its quality factor was not changed upon cooling. At each temperature, the magnitude of the resonance signal under study was calibrated versus a reference sample ($MgO:Mn^{2+}$) situated outside the Dewar tube.

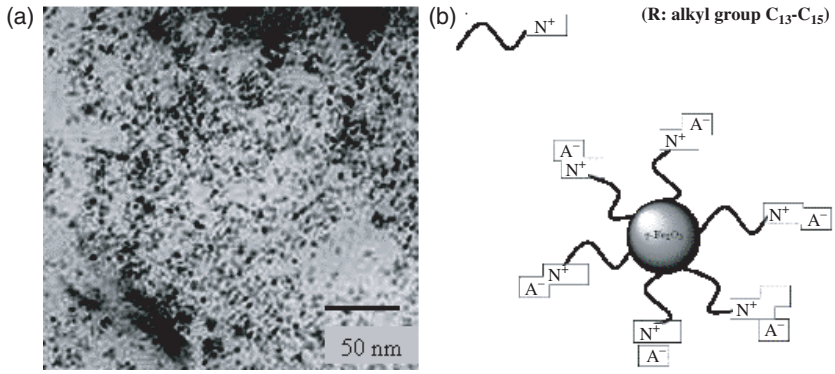

Figure 1. (a) TEM picture of the ferrofluid. (b) Schematic of surface functionalized γ-Fe_2O_3 nanoparticles.

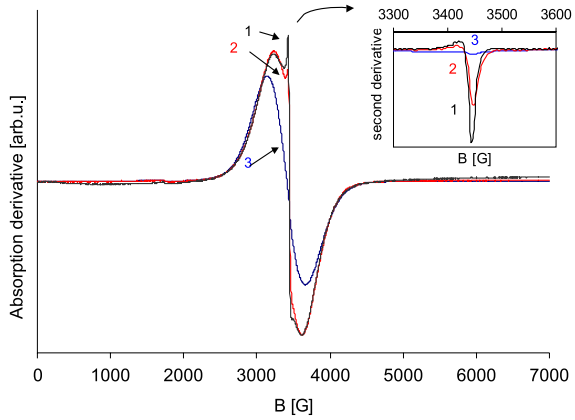

Figure 2. The EMR signal in the ferrofluid diluted in toluene at $T = 295$ K. The degree of dilution (by weight) is 1:6000 (1), 1:200 (2) and 1:6 (3). The spectra are normalized to the same intensity (double integrated area). Inset: the derivative of the EMR signal demonstrating the narrow peak.

The longitudinal relaxation time (T_1) was measured by a modulation technique using the homemade apparatus by detecting the longitudinal magnetization component oscillating at the modulation frequency of 1.6 MHz [21]. Both 'phase' and 'amplitude' versions were employed; in the latter case, the diphenylpicrylhydrazyl (DPPH) was used as a reference sample.

Typical EMR signals at room temperature ($T = 295$ K) are shown in figure 2. The signal can be described approximately as a sum of two lines, a broad one with a peak-to-peak width of about 500 G and a narrow one with a width of about 30 G. The narrow line has a g-factor of $g \approx 2$; it can be seen more clearly in the derivative of the EMR signal (that is the second derivative of the EMR absorption; see inset in figure 2). This narrow signal is observed in well-diluted samples; with an increase in the nanoparticle concentration, it becomes broader, lower in amplitude and not well resolved.

The EMR spectra taken at different temperatures are shown in figure 3. One can see that with a decrease in temperature the broad signal shifts toward lower fields and its width increases.

The temperature dependences of the line shift, $B_0 - B_0(T)$, and peak-to-peak width ΔB_{pp} for the γ-Fe_2O_3 suspension in the polymer matrix are presented in figure 4(a). Here $B_0(T)$

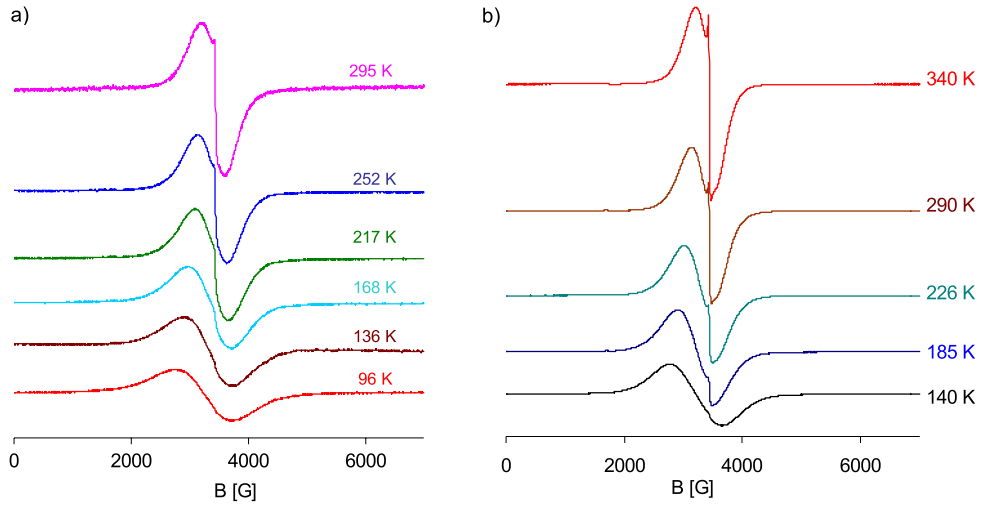

Figure 3. EMR in γ-Fe_2O_3 suspensions in the polymer matrix (a) and toluene (b) at different temperatures.

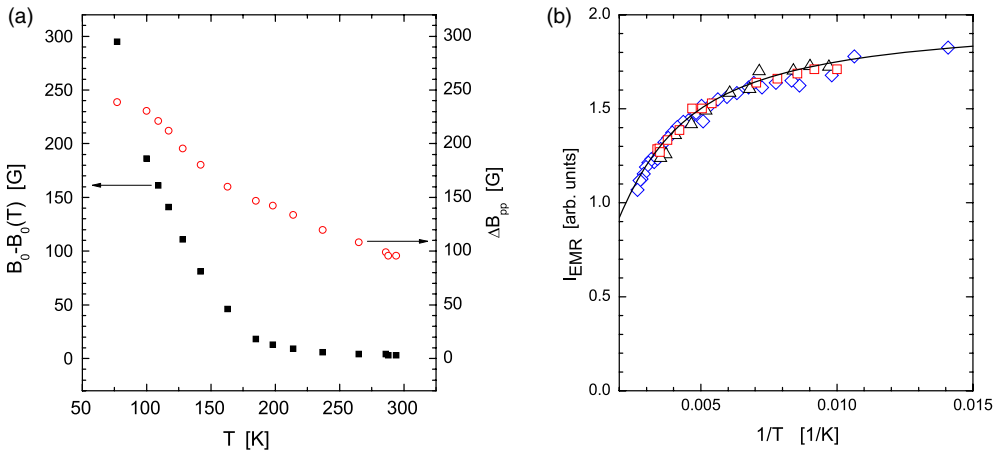

Figure 4. (a) Temperature dependences of the EMR line shift (filled squares, left scale) and width (open circles, right scale) for the γ-Fe_2O_3 suspension in the polymer matrix. (b) The EMR intensity in the nanoparticle systems diluted in polymer (squares), diluted in toluene (triangles) and in ferrofluid as it is (diamonds). The data obtained with the different samples are normalized to the same value at 295 K. The solid line is the model with $\eta \equiv \mu B_0/k_B = 800$ K, see equation (1).

is the resonance field determined as the point where the absorption derivative equals zero at the temperature T, and $B_0 = 3442$ G represents its asymptotic value at high temperatures. The EMR intensity, I_{EMR}, calculated through double integration of the absorption-derivative spectrum is shown in figure 4(b). In both diluted and dense ferrofluids the EMR intensity follows the same temperature dependence: as the temperature decreases, I_{EMR} increases and tends to some constant value.

We made an attempt to find evidence for ferromagnetic blocking, frequently observed in magnetic nanoparticles at low enough temperatures (see, for example, [1, 12, 17, 22, 23]). The EMR intensity was measured under conditions of zero field cooling (ZFC). Each point in the

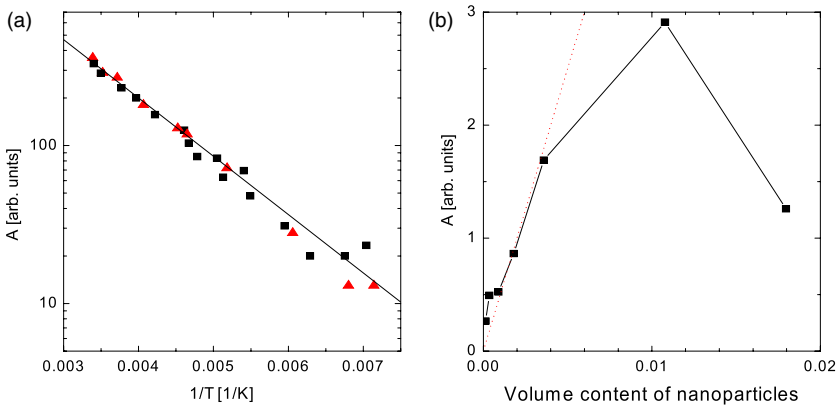

Figure 5. Properties of the narrow spectral component. (a) Magnitude of the narrow component in polymer (squares) and toluene (triangles) matrices. The solid line is $\exp(-E_a/k_B T)$, with $E_a/k_B = 850$ K. (b) Magnitude of the narrow line versus nanoparticle concentration in toluene ($T = 295$ K). The solid line connects the experimental points. The dotted line shows a linear dependence at low concentration.

temperature dependence was obtained after previously heating the sample up to 300 K and subsequent cooling to the desired temperature at $B = 0$; then the EMR spectrum was recorded during the first up-field sweep. No difference in the EMR intensity was found in comparison to the field cooling (FC) procedure, indicating absence of blocking in our experiments. This can be explained by relatively low values of the effective anisotropy fields, $B_a \ll B_0 \approx 3.5$ kG. Note that blocking of maghemite nanoparticles in magnetic fields of several kG was only observed at $T < 40$ K [12, 23].

Opposite to the broad signal behaviour, the narrow signal remains at the same field whereas its amplitude decreases steeply with decrease in temperature (see figure 5(a)). The shape of the narrow component (both in the first derivative and second derivative presentations) was thoroughly analysed and found to be temperature independent, at least in its central (peak-to peak) part. This finding enables one to consider the data presented in figure 5(a) as the temperature dependence of the narrow line intensity.

To check whether the narrow component is related to the organic groups on the nanoparticle surface, we ran the EMR spectra of the systems containing similar surface-modified silica nanoparticles, fabricated by the same method [20]. No signal was observed. Note that such double-feature spectra were previously reported for dispersed maghemite nanoparticles [9, 11], as well as various superparamagnetic and exchange-coupled clusters in solid matrices [13, 14].

The dependence of the narrow line magnitude on the nanoparticle volume content (c) in liquid toluene solutions is shown in figure 5(b). All data are normalized to the sample volume. At low concentrations ($c \leqslant 4 \times 10^{-3}$), the peak magnitude is proportional to c, whereas the pronounced drop occurs at $c > 0.01$, accompanied by a 10–20% increase in the peak-to-peak line-width (not shown in the figure). In the concentrated ferrofluid, the narrow feature is not observable.

The longitudinal relaxation time T_1 corresponding to the observed EMR spectrum was measured by the modulation technique with longitudinal detection [21]. A value of $T_1 = (10 \pm 3)$ ns was obtained for the concentrated samples in the temperature range of 77–300 K, whereas a T_1 twice as long was found in the central part of the spectrum for the diluted solid sample.

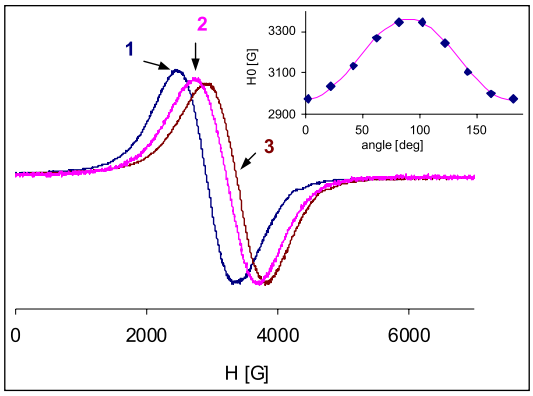

Figure 6. The EMR at 77 K in the samples diluted in toluene after ZFF (trace 2) and FF with $\boldsymbol{B}_{\rm fr} = 7$ kG and $\beta = 0$ (trace 1) and $\beta = \pi/2$ (trace 3). Inset: the line position in dependence on the orientation of the measuring field $\boldsymbol{B}_{\rm m}$ relative to the direction of the freezing field $\boldsymbol{B}_{\rm fr}$. Dots are experimental points and the solid trace corresponds to $\cos^2\beta$.

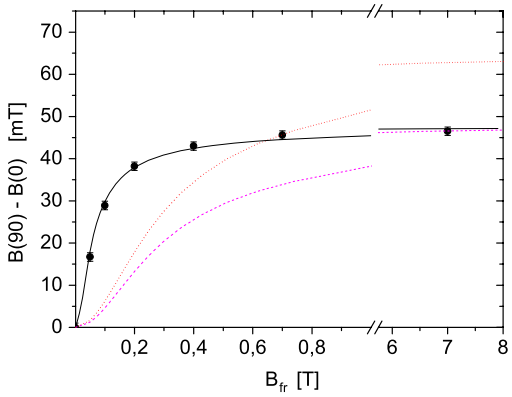

Figure 7. Difference between the resonance fields B_0 ($\beta = 90°$) and B_0 ($\beta = 0$) after the FF procedure versus the freezing field $B_{\rm fr}$. Black squares, experiment at 77 K; curves, calculation based on equation (16) with $\eta \equiv \mu B_0/k_{\rm B} = 4300$ K, $B_{\rm a} = 800$ G (solid trace); $\eta = 800$ K, $B_{\rm a} = 2040$ G (dotted); and $\eta = 800$ K, $B_{\rm a} = 2380$ G (dashed).

Following the method suggested in [8], we studied the effect of alignment under field-freezing (FF) conditions. Samples diluted in toluene (freezing temperature $T_{\rm fr} = 180$ K) were cooled and frozen at the external magnetic field $\boldsymbol{B}_{\rm fr}$. Then the frozen sample was rotated versus the vertical axis, so the measuring field, $\boldsymbol{B}_{\rm m}$, made an angle β with the direction of the alignment related to $\boldsymbol{B}_{\rm fr}$. The EMR spectra observed after the FF procedure at both $\beta = 0$ and $\beta = \pi/2$ are presented in figure 6, together with the spectrum corresponding to zero-field freezing (ZFF) performed at $\boldsymbol{B}_{\rm fr} = 0$. The measuring temperature was low enough (77 K), and only the broad spectral component was observed. The angular dependence of the line position is shown in the inset of figure 6. As one can see, the resonance line in the FF sample is shifted from the position of the ZFF experiment toward lower fields if the measuring field, $\boldsymbol{B}_{\rm m}$, is parallel to $\boldsymbol{B}_{\rm fr}$ ($\beta = 0$) or toward higher fields at the perpendicular orientation ($\beta = \pi/2$).

This shift depends on the freezing field magnitude, demonstrating gradual saturation for fields higher than 4 kG (see figure 7). No FF effect was observed in nanoparticles dispersed in a solid polymer matrix.

The orientation dependence of the line position demonstrates a maximum at 90° and can be well fitted with the dependence $\cos^2 \beta$ (see the inset in figure 6) similar to the results obtained in [8]. According to [8], this indicates predominance of the axial type of magnetic anisotropy (in the case of cubic magnetocrystalline anisotropy, one would observe the dependence with two maxima). This issue will be discussed below (section 3).

3. Theory and discussion

The samples under study are ensembles of small ($d \approx 5$ nm) particles of γ-Fe_2O_3 embedded into non-magnetic matrix (liquid or solid). The Curie temperature of bulk maghemite, $(T_C)_{bulk} = 860$ K [8], is higher than the measurement temperatures (77–380 K), and the nanoparticles are formally in the ferrimagnetic single-domain state. The anisotropy field B_a can be considered to be much lower than the external field B under EMR conditions. In this case, the direction of the effective field $\boldsymbol{B}_e$ practically coincides with the direction of $\boldsymbol{B}$, and, in the ground state, all individual magnetic moments $\boldsymbol{\mu}$ are aligned along the same direction. This entirely polarized state is, however, disturbed by thermal fluctuations. The magnetic energy of a nanoparticle, $U_m = -(\boldsymbol{\mu} \cdot \boldsymbol{B})$, is comparable with $k_B T$ (where k_B is the Boltzmann constant); as a result the direction of $\boldsymbol{\mu}$ fluctuates, giving rise to specific superparamagnetic properties.

The theory of magnetic dynamics and EMR in superparamagnetic objects was developed in [3–5]. Starting from the Landau–Lifshitz (LL) equation, Raikher and Stepanov (RS) [3, 4] took into account thermal reorientations of $\boldsymbol{\mu}$, and using the approximation $B_a \ll B$, obtained the expression for the magnetic resonance absorption. The main result of the RS theory is the effective reduction (so-called 'dressing') of the anisotropy field.

According to the model, the EMR spectrum in the superparamagnetic regime strongly depends on temperature. In the low-temperature limit ($\xi \equiv \mu B / k_B T \gg 1$), random distribution of the anisotropy axes results in huge inhomogeneous broadening (with an overall width of 1.5 B_a). The theory [3, 4] predicts for this case a specific, highly asymmetric line shape typical for FMR in powdered samples. As the temperature increases, the width and asymmetry of the spectrum decreases progressively. Finally, the EMR spectrum is expected to collapse into a single Lorentzian line centred at $B_0 = \omega/\gamma$, where ω is the operating frequency and γ is the gyromagnetic ratio. At further heating, this line broadens due to the increase of the relaxation rate. Numerically calculated spectra for a set of typical parameters are presented in [3, 4].

However, many of the reported experimental data hardly agree with these predictions. In particular, the EMR spectra of maghemite nanoparticles of various size and in various matrices were found to be different from the RS theoretical calculations, especially at low temperatures. The same is true for our data as well: as it is seen from figure 3, the spectra become broader and more symmetric as temperature decreases, in contradiction with the RS model. Besides, the line is shifted to lower fields upon cooling. Finally, the additional narrow line is observed at $B \approx B_0$, with the magnitude strongly dependent on temperature. Similar features were reported previously for many nanoparticle systems (see for example [6–19]). Various explanations of these 'anomalies' have been proposed, including accounting for specific features of spins belonging to a particle surface. Below we will discuss these issues, as well as the FF phenomena and effect of inter-particle interactions, in more detail.

Before proceeding further, let us estimate the value of the magnetic moment $\boldsymbol{\mu}$ of an individual nanoparticle. In principle, this value could be calculated as $\mu = V M_s$, where V is the particle volume and M_s is its saturated magnetization. However, M_s in nanoparticles can deviate from the bulk value of 400 emu cm^{-3} [17]. The EMR spectra provide an opportunity to estimate $\boldsymbol{\mu}$ directly from the temperature dependence of the EMR intensity.

As was mentioned above, nanoparticles dispersed in a non-magnetic matrix can be considered as superparamagnetic objects with a very large spin $S \sim 10^3$. The temperature dependence of their static magnetic susceptibility obeys the formula

$$\chi(T) = CL(\xi), \tag{1}$$

where C is a temperature-independent coefficient and $L(\xi) = \coth(\xi) - 1/\xi$ is the Langevin function. Under EMR conditions, the specific form of the $\chi(T)$ dependence is determined mainly by the value of $\boldsymbol{\mu}$. Thus, taking into account that the susceptibility is proportional to the EMR intensity (double integrated area under the EMR line), one can determine $\boldsymbol{\mu}$ from the experimental data (figure 4(b)).

The best fit of the experimental dependence with equation (1) is obtained at $\eta = (800 \pm 100)$ K, where $\eta \equiv \mu B_0/k_B$ is introduced, with $B_0 = 3.44$ kG. Thus the magnetic moment of an individual particle amounts to $\sim 3.4 \times 10^3$ Bohr magnetons, corresponding to the total spin S of 1700. For $M_s = 400$ emu cm^{-3}, this corresponds to a nanoparticle with the diameter of ~ 5.4 nm which is close to the value of d estimated from TEM studies.

Let us discuss now the origin of the narrow feature, which is clearly seen at the centre of the EMR spectra in both liquid and solid diluted samples at high enough temperatures. As seen in figure 5(a), its amplitude decreases upon cooling, approximately obeying the Arrhenius law with an activation energy of about 850 K (in k_B units). On the other hand, the shape and the width of the narrow line are found to be practically temperature independent. This suggests that the temperature dependence of the peak magnitude shown in figure 5(a) reflects the behaviour of the integrated intensity, at least for the central (peak-to-peak) part of the narrow component.

Berger *et al* [13, 14] suggested that the narrow component observed in the EMR spectra of superparamagnetic objects is due to contributions from very small particles. If $\xi \ll 1$, that would lead to strong reduction of the effective anisotropy field and collapse of the spectrum into a single Lorentzian line at $g = 2$. Detailed analysis shows, however, that this scenario does not describe our case. According to [13, 14], the width of the narrow component would increase rapidly upon cooling due to lessened thermal averaging [3, 4]; by contrast, the width of the narrow line shown in figure 3 remains constant until its eventual disappearance at low temperatures. Nevertheless, the Berger–Klyava model [13, 14] cannot be rejected ultimately.

Another explanation was proposed by Gazeau *et al* [9], referring to the RS theory modified by taking into account the 'inhomogeneous broadening' caused by the dependence of the FMR frequency on the angle, ψ, between the magnetic moment $\boldsymbol{\mu}$ and magnetic field $\boldsymbol{B}$ [24, 25]. Unfortunately, the detailed theory was not presented in [9, 24, 25], except for the case of $B = 0$. Below, we suggest a model, which, in our opinion, is compatible with this idea. We will show that the anisotropy terms are cancelled in the first order at $\psi = \pi/2$, and the narrow component arises at this excited state with the probability of $\exp(-\mu B_0/k_B T)$, in fair agreement with figure 5(a).

Whatever the origin of the narrow spectral component may be, it experiences dipolar magnetic fields produced by the particles. To estimate this effect, let us use the statistical theory of the dipole–dipole broadening of the EPR in magnetically diluted spin systems [26], which can be applied as a crude approximation to our case. According to [26], a Lorentzian line-shape is predicted, with the peak-to-peak width of its derivative being

$$\delta_{pp}^{(1)} = \frac{16\pi^2}{27} Mc, \tag{2}$$

and the full width at half-height of the second derivative central peak

$$\delta_{1/2}^{(2)} = \frac{16\pi^2}{27\sqrt{3}} Mc. \tag{3}$$

For example, for the highest c of 0.018 presented in figure 5(b), one gets $\delta^{(2)}_{1/2} \cong 24$ G, whereas the experimentally observed concentration-dependent part of the broadening does not exceed 3–4 G. This discrepancy shows that the dipolar fields contribute mostly to the non-observable distant wings rather than to the peak-to-peak interval, and the real shape of the dipolar-broadened line is not Lorentzian. Such a case is typical for a non-random space distribution of magnetic entities with a tendency to aggregation. In aggregates, the dipolar fields are much stronger than those at mean distances. Thus, the narrow spectral component is provided only by 'free' particles, which are not coupled into dipolar clusters. According to the above estimations, the fraction of free particles in our suspensions does not exceed 10–20%. The role played by particle aggregation will be discussed later.

Let us now fit, at least qualitatively, the shape of the observed EMR spectra, including characteristic temperature evolution of both the narrow and broad components. Simultaneous existence of these two distinct spectral features is difficult to explain in the frames of the RS theory [3, 4], which suggests averaging over all possible states due to fast rotary diffusion of the magnetic moment. To overcome this problem, we assume, as a likely hypothesis, that thermally activated jumps of $\boldsymbol{\mu}$ between different orientations are not fast enough, and the Larmor precession can be definitely distinguished at each particular angle ψ between $\boldsymbol{\mu}$ and $\boldsymbol{B}$. In such a case, the observed FMR spectrum can be represented as a sum of the signals corresponding to various ψ, with proper account of their probabilities.

The bulk anisotropy of γ-Fe_2O_3 is cubic, with $K_c \sim -4.7 \times 10^4$ erg cm^{-3} [27]. This rather low value cannot explain the observed width of the EMR spectrum, especially at low temperatures. However, the particles may have additional anisotropy that can be caused by small deviations from the spherical shape combined with surface effects [8]. Let us introduce the axial anisotropy field $\boldsymbol{B}_a$ as the fitting parameter. In what follows, the high-field approximation,

$$B \gg B_a \tag{4}$$

is adopted, so the direction of the effective field (the precession axis) practically coincides with $\boldsymbol{B}$.

We start with the well-known expression for the energy of an anisotropic ferromagnet in a magnetic field:

$$U = -(\boldsymbol{\mu} \cdot \boldsymbol{B}) - KV \cos^2 \varphi, \tag{5}$$

where $K = B_a M/2$ is the specific anisotropy energy and φ is the angle between $\boldsymbol{\mu}$ and the anisotropy axis $\boldsymbol{n}$. Applying the standard master equation for the classical magnetic moment and neglecting the relaxation, it can be shown [28] that the precession of $\boldsymbol{\mu}$ under the condition of equation (4) occurs at the frequency

$$\omega_{\psi,\theta} = \omega_0 + \gamma B_a \cos\psi \cdot P_2(\cos\theta), \tag{6}$$

where $\omega_0 = \gamma B$; $P_2(y) = (3y^2 - 1)/2$ is the Legendre polynomial and θ is the angle which $\boldsymbol{B}$ makes with the anisotropy axis. The expression of equation (6) differs from the standard FMR by a factor of $\cos\psi$ which accounts for deviation of $\boldsymbol{\mu}$ from its ground-state direction ($\psi = 0$) due to thermal excitation and describes the superparamagnetic behaviour.

We consider this frequency as the centre of an individual resonance line ('spin packet'), which is related to the given value of ψ. The corresponding resonance field is

$$B_{\psi,\theta} = B_0 - B_a \cos\psi \cdot P_2(\cos\theta), \tag{7}$$

where $B_0 = \omega/\gamma$, and ω is the microwave frequency.

At this stage, let us switch to the notations commonly used in the field of EPR. Namely, we denote $\cos\psi = -m/S$, where m is the magnetic quantum number determining the projection

of the total spin S of the particle on the $\boldsymbol{B}$ direction. Further, let us introduce the parameter D, defined through $\gamma B_a = -2DS$. In these notations, equations (5)–(7) become very similar to the equations describing a paramagnetic spin system with the standard axially symmetric spin Hamiltonian:

$$\hat{H}/\hbar = \gamma\left(\vec{B}\cdot\vec{S}\right) + DS_n^2, \tag{8}$$

where D is the crystal-field parameter commonly used in EPR.

In high-field approximation, the resonance field corresponding to this Hamiltonian is:

$$B_{m,\theta} = B_0 + \frac{1}{\gamma}(2m+1)\,DP_2(\cos\theta)\,. \tag{9}$$

Comparing equations (8) and (9) with equations (5) and (7), one can see that the 'quantization' description fully coincides with the 'ferromagnetic' formalism at S, $m \gg 1$. In fact, the spin Hamiltonian, equation (6), describes the ground spin multiplet of the particle considered as a giant exchange cluster.

To calculate the spectra, we take into account the probabilities of the allowed $(m, m+1)$ transitions [26] as

$$W_{m,\theta} = Ag(B - B_{m,\theta})\,[S(S+1) - m(m+1)]\,, \tag{10}$$

and the equilibrium (Boltzmann) distribution of populations on the magnetic sublevels,

$$\rho_{m,\theta} = Z_\rho^{-1}\exp\left(\frac{-E_{m,\theta}}{k_B T}\right). \tag{11}$$

Here A is the proportionality factor, $g(B - B_{m,\theta})$ is the form-factor of the resonance line at the transition involved and Z_ρ is the partition function. In our calculations either Lorentzian or Gaussian shapes were tested, with the corresponding value of the half-width δ as a fitting parameter.

The resonance absorption is proportional to the population difference at the adjacent levels, $\rho'_{m,\theta} = \partial\rho_{m,\theta}/\partial m$. As a result, the shape of the EMR absorption spectrum for an assembly of nanoparticles with random distribution of the anisotropy axes reads:

$$G(B - B_0) = \int_0^\pi \sin\theta\,\mathrm{d}\theta \int_{-S}^{S} W_{m,\theta}\rho'_{m,\theta}\,\mathrm{d}m. \tag{12}$$

Before proceeding further, let us discuss distinctions between the approach described above and the classical FMR consideration. Superparamagnetic nanoparticles can be considered as an intermediate case between ordinary ferromagnets and exchange coupled paramagnetic clusters (or molecular magnets). In the ferromagnetic case, spin systems always remain in their ground state; in the exchange cluster, this situation corresponds to the high-spin ground multiplet separated from the upper one by a gap of about $JS \gg k_B T$, where J is the exchange integral. Since the spin wave energy is inversely proportional to the square of the particle diameter [29], this picture can be well justified for our case. Note that a similar 'quantization' approach was employed previously when interpreting magnetization [30, 31] and nuclear spin relaxation [32] in superparamagnetic samples.

The results of the quantization approach differ from the predictions of the RS theory [3, 4]. In the latter case, averaging is performed over all ψ values, suggesting validity of the LL equation for a magnetic nanoparticle as a whole. This means, in particular, that the longitudinal and transverse relaxation times (T_1 and T_2) are assumed to be nearly equal and determined by the LL relaxation parameter. Unlike this, equations (11)–(12) include the summation over all $(m, m+1)$ transitions, assuming that each of them is well distinguished and characterized by characteristic T_1 and T_2 values, according to the Bloch equations. This suggestion is supported

by the measured value of $T_1 = 10$–20 ns, which exceeds considerably the value of $T_2 \sim 2$ ns estimated from the width of the narrow feature in the diluted samples.

An important consequence of the quantization approach is the appearance of the narrow spectral component in the centre of the EMR spectrum. This component results from the states in the vicinity of $\psi = \pi/2$ which are not affected by the anisotropy term (see equations (7), (9)), and thus not broadened by a random distribution of the symmetry axes. Since the energy of these states lies well above the ground level, the intensity of the narrow feature decreases exponentially upon cooling. Note that similar thermally activated double-pattern spectra have also been observed in very different systems, such as some glasses doped with paramagnetic ions [2, 13, 14] and magnetically dilute $LaGa_{1-x}Mn_xO_3$ at intermediate Mn concentrations [33], and were ascribed to spin clusters. This similarity in EMR spectra and temperature behaviour may have significant physical meaning, revealing continuous transfer from the exchange coupled spin clusters in diamagnetic host lattices to superparamagnetic nanoparticles.

Another effect to be accounted for in our simulations is the experimentally observed broadening and shift of the EMR line to lower fields upon cooling (see figures 3 and 4(a)). These features are typical for magnetic nanoparticles (see, for example, [2, 8, 12, 15, 34]); as a rule, they are ascribed to surface phenomena. The surface effects in magnetic nanoparticles are intensively discussed in the literature. The specific surface-related magnetic anisotropy, which combines surface effects with deviation from a spherical shape, was first introduced by Néel [35] and used later to interpret the EMR data [8]. The shift of the EMR line upon cooling was ascribed to the 'exchange anisotropy' arising at the interface between ferro- and antiferromagnetic (or spin–glass) layers [36, 37]. In this context, Kodama and Berkowitz [38] performed sophisticated model calculations for γ-Fe_2O_3 nanoparticles and proved the spin–glass-like arrangement of surface spins. Specific magnetic properties of spins adjacent to the particle surface were also studied by numerical calculations in [39]. Some experimental evidence for surface spin glass was reported in [12, 23].

Without rejecting these plausible mechanisms, we would like to suggest one more model, which can even be applied to strictly spherical particles. Our model is based on the existence of the strong radial field acting on spins belonging to the particle surface. This field is due to the electric field gradient (EFG) caused by lack of the outer oxygen in the first coordination octahedron surrounding the magnetic ion (Fe^{3+}, for example). Our estimations using the point-charge model showed that the crystalline anisotropy parameter on the surface, D_s, can exceed the anisotropy parameter, D, of the bulk by about two orders of magnitude. If the exchange interactions were absent, this would lead to a considerable shift, $\Delta B = B - B_0$, of the resonance field for the surface spins. In the first-order (linear) approximation, the shift $\Delta B^{(1)}$ is proportional to $D_s m P_2(\cos\theta')$ (see equation (9)), where θ' is the angle between $\boldsymbol{B}$ and the local anisotropy axis at a given point on the surface. In the case of the isotropic exchange interaction, this shift averages to zero for spherical particles. In the real situation, however, particle surfaces are not smooth at the atomic scale; this would lead to the broadening of the spectra. Since the magnitude of the shift is proportional to $|m|$, it is natural to suggest that the same is true for the width of the Gaussian distribution related to the random imperfections on the surface, as well as variations in the particle shape. As a result, one can assume for the partial line-width at the transition $(m, m+1)$:

$$\delta(m) = \delta_0 + a\frac{|m|}{S}, \tag{13}$$

where the initial line-width δ_0 and factor a are fitting parameters.

In contrast to the linear approximation, the second-order shift $\Delta\boldsymbol{B}^{(2)}$ is not averaged to zero by the exchange interactions, and leads to the non-zero first spectral moment in the

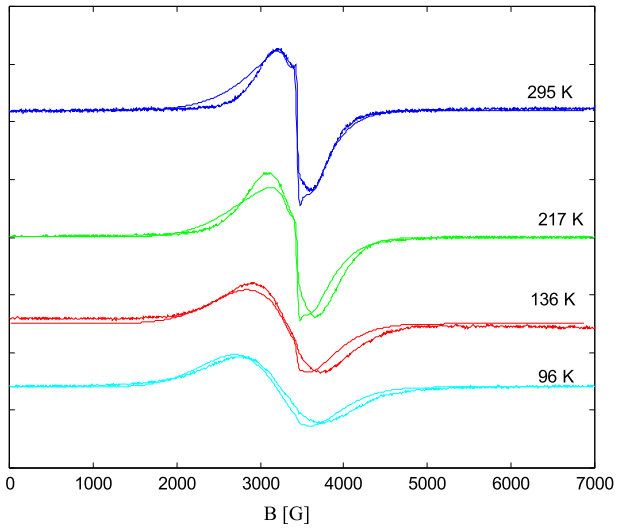

Figure 8. Fitting of the experimental data (nanoparticles in the polymer matrix) with equations (9)–(12) and (13)–(15). Solid traces, experiment; dotted traces, theory. Temperatures are indicated in the figure.

resulting spectrum, i.e. a shift of the line to lower fields. It is appropriate to suggest (see, for example, [26]) that the averaged second-order shift is proportional to m^2 and can be represented as

$$\langle \Delta \boldsymbol{B}^{(2)} \rangle = -C \frac{{D_s}^2}{\gamma^2 \boldsymbol{B}_0} \left(\frac{m}{S} \right)^2 \tag{14}$$

where $\langle \cdots \rangle$ denotes averaging over all spins of the particle and $C > 0$ is the numerical coefficient which is proportional to relative number, N_{ss}/N, of surface spins. Note, that N_{ss}/N is inversely proportional to the particle size and amounts to 0.2–0.3 for $d \sim 5$ nm.

Based on the arguments mentioned above, we assume that the resonance field of the $(m, m+1)$ transition can be expressed as

$$\boldsymbol{B}'_{m,\theta} = \boldsymbol{B}_{m,\theta} - c \left(\frac{m}{S} \right)^2 \tag{15}$$

where c is the fitting parameter.

Upon cooling, the lowest energy levels with $m \to -S$ become more and more populated, thus resulting, according to equations (13)–(15), in both broadening and shift of the EMR line, as observed in the experiment.

Using equations (13) and (15), we fit the experimental spectra of nanoparticles dispersed in solid polymer (see figure 8).

The parameters employed at this fitting were: $\eta = 800$ K (this corresponds to $S = 1700$); $\boldsymbol{B}_a = 600$ G; $a = 640$ G; $c = 560$ G; the Gaussian line shapes were used as $g(\boldsymbol{B}_{m,\theta} - \boldsymbol{B}_0)$. According to the observed concentration dependence of the narrow component (figures 2 and 5(b)), the value of $\delta_0 = 30$ G was ascribed to 'free' particles, whereas $\delta'_0 = 200$ G was used for aggregates subjected to the inter-particle dipole–dipole interactions. The best fit was obtained with the fraction of the free particles assumed to be of 20%. As one can see, the calculated spectra agree qualitatively with the experimental ones.

Let us discuss now the field freezing (FF) experiments (section 2, figures 6, 7). Our data are consistent with those obtained previously by Gazeau *et al* with maghemite nanoparticles

in anionic ferrofluid [8]. In both cases, a specific angular dependence of the resonance field after the FF procedure was observed. As can be seen from figure 6, this dependence has only one maximum in the range of 0°–180° and can be well fitted by a simple expression $\cos^2\beta$. Such behaviour indicates uniaxial anisotropy in contrast to cubic symmetry known for bulk γ-Fe_2O_3. Gazeau *et al* [5] suggested that this anisotropy is related to individual nanoparticles. Since the estimations showed that the observed anisotropy cannot be assigned to the particle shape alone, the authors of [5] assigned it to the surface effects combined with a deviation from spherical shape, as predicted by Néel [35]. In our opinion, however, this assumption can hardly be accepted. Consider this issue in more detail.

According to [4], the equilibrium orientational distribution $f(\theta)$ of the anisotropy axes relative to $\boldsymbol{B}_{\rm fr}$ results from competition between the magnetic and anisotropy energy of a nanoparticle with thermal energy ($k_{\rm B}T$). The explicit formula for $f(\theta)$ is given in [4]. Following the ideas of [4, 40], Gazeau *et al* [8] obtained the following expression for the difference between the line positions at $\boldsymbol{B}_{\rm m} \perp \boldsymbol{B}_{\rm fr}$ ($\beta = 90°$) and $\boldsymbol{B}_{\rm m} \parallel \boldsymbol{B}_{\rm fr}$ ($\beta = 0$):

$$\boldsymbol{B}_0(90) - \boldsymbol{B}_0(0) = \tfrac{3}{2}\int_0^{\pi/2} f\,(\theta)\,P_2(\cos\theta)\sin\theta\,{\rm d}\theta. \tag{16}$$

We made an attempt to fit the experimental dependence of $\boldsymbol{B}_0(90^0) - \boldsymbol{B}_0(0)$ on $\boldsymbol{B}_{\rm fr}$ (see figure 7) using equation (16) with $T_{\rm fr} = 180$ K. The best fit is shown by the solid curve. Parameters determined from this fitting procedure are: $\eta \equiv \mu\boldsymbol{B}_0/k_{\rm B} = (4300 \pm 400)$ K and $\boldsymbol{B}_{\rm a} = (800 \pm 100)$ G. Though the obtained value of $\boldsymbol{B}_{\rm a}$ is close to the upper limit determined by the observed width of the EMR spectra, the value of η exceeds dramatically any reasonable estimation. On the other hand, the curves calculated with a realistic $\eta = 800$ K (dotted and dashed lines at figure 7) disagree strongly with the experimental data. Note that the same problem arises if one analyses the data of Gazeau *et al* [8, 9]. In fact, the reported value of $\boldsymbol{B}_{\rm a} = 2.2$ kG for $d = 4.8$ nm [8] should lead to an extremely asymmetric and very broad spectrum, in strong disagreement with the experiment.

Thus, the model of alignment based on [4, 8] and equation (14) does not provide a good quantitative description of the experimental data. In fact, the best-fit value of η corresponds to a 5–6 times enlarged magnetic moment of the particle, clearly pointing to some collective effects (aggregation) probably caused by inter-particle interactions. As an example, dipolar chain formation can be suggested which is typical for ferrofluids [41]. In such a case, both the FF shift value and the $\cos^2\beta$ angular dependence can be readily explained by taking into account the dipolar fields induced by the neighbouring particles in the aligned chains. Our estimations show that the dipolar fields existing in such a chain agree well with the experimental data (figures 6, 7). For more details see [42].

4. Conclusion

In conclusion, the EMR spectra and longitudinal spin relaxation have been studied in both concentrated magnetic fluid and diamagnetically diluted objects containing 5 nm maghemite nanoparticles. The spin-relaxation time T_1 is found to be in the order of 10 ns and temperature independent at $T = 77$–300 K. The EMR spectra consist of broad and narrow components, the latter having a temperature-independent g-factor and revealing a thermally activated intensity with $E_{\rm a}/k_{\rm B} \cong 850$ K. In contrast, the broader component shows considerable broadening and shifting to lower fields upon cooling. This behaviour, as well as a nearly symmetrical shape of the broad line, cannot be satisfactorily described by the standard RS theory [3, 4]. It is shown that the strong radial anisotropy experienced by surface spins may be partially responsible for the shift and broadening of the observable EMR spectrum through the surface–bulk exchange interaction.

To explain the appearance and approximately exponential temperature dependence of the narrow spectral component at $g \approx 2$, we propose the hypothesis of independent contributions from energy states differing by magnetic quantum numbers, m. At small $|m|$ (corresponding to nearly a right angle between $\boldsymbol{\mu}$ and $\boldsymbol{B}$ in the classical description), the anisotropy-related inhomogeneous broadening disappears, giving rise to a narrow spectral component with an intensity proportional to $\sim \exp(-\mu \mathrm{B}/k_{\mathrm{B}}T)$. This 'quantization' approach enables one to fit, at least qualitatively, the shape of the observed spectrum in the whole temperature range studied (77–295 K).

Experiments on freezing of the liquid samples in the magnetic field $\boldsymbol{B}_{\mathrm{fr}}$ (the FF procedure) provide evidence for axial anisotropy in the resulting EMR spectrum. Quantitative analysis showed that these data cannot be described by single-particle axial anisotropy and suggested the influence of collective effects, such as chain formation due to inter-particle dipole–dipole interactions. The tendency to particle aggregation is also confirmed by the dependence of the narrow line parameters on the degree of diamagnetic dilution.

Acknowledgments

The work was partly supported by National Science Foundation (NSF) CREST Project HRD-9805059, NSF PREM grant no DMR-0611430, Russian Foundation for Basic Research (grant 05-02-16371) and Program P-03 for Basic Research of Russian Academy of Sciences.

The authors are greatly indebted to F S Dzheparov for help with theoretical calculations and fruitful discussions and to R R Rakhimov and V V Demidov for help with EMR experiments.

References

[1] Dormann J L, Tronc E and Fiorani D 1997 *Adv. Chem. Phys.* **98** 283
[2] Kliava J and Berger R 2003 *Recent Res. Dev. Non-Cryst. Solids* **3** 41
[3] Raikher Yu L and Stepanov V I 1992 *Sov. Phys.—JETP* **75** 764
[4] Raikher Yu L and Stepanov V I 1994 *Phys. Rev.* B **50** 6250
[5] de Biasi E, Ramos C A and Zysler R D 2003 *J. Magn. Magn. Mater.* **262** 235
[6] Valstyn E P, Hanton J P and Morrish A H 1962 *Phys. Rev.* **128** 2078
[7] Nagata K and Ishihara A 1992 *J. Magn. Magn. Mater.* **104–107** 1571
[8] Gazeau F, Bacri J C, Gendron F, Perzynski R, Raikher Yu L, Stepanov V I and Dubois E 1998 *J. Magn. Magn. Mater.* **186** 175
[9] Gazeau F, Shilov V, Bacri J C, Dubois E, Gendron F, Perzynski R, Raikher Yu L and Stepanov V I 1999 *J. Magn. Magn. Mater.* **202** 535
[10] Respaud M, Goiran M, Broto J M, Yang F H, Ould Ely T, Amiens C and Chaudret B 1999 *Phys. Rev.* B **59** R3934
[11] Prodan D, Grecu V V, Grecu M N, Tronc E and Jolivet J P 1999 *Meas. Sci. Technol.* **10** L41
[12] Koksharov Yu A, Gubin S P, Kosobudsky I D, Yurkov G Yu, Pankratov D A, Ponomarenko L A, Mikheev M G, Beltran M, Khodorkovsky Y and Tishin A M 2000 *Phys. Rev.* B **63** 012407
[13] Berger R, Kliava J, Bissey J-C and Baietto V 2000 *J. Appl. Phys.* **87** 7389
[14] Berger R, Bissey J-C, Kliava J, Daubric H and Estournes C 2001 *J. Magn. Magn. Mater.* **234** 535
[15] Upadhyay R V, Parekh K and Mehta R V 2003 *Phys. Rev.* B **68** 224434
[16] Winkler E and Zysler R D 2004 *Phys. Rev.* B **70** 174406
[17] Dutta P, Manivannan A, Seehra M S, Shah N and Huffman G P 2004 *Phys. Rev.* B **70** 174428
[18] Wiekhorst F, Shevchenko E, Weller H and Kötzler J 2004 *J. Magn. Magn. Mater.* **272–276** 1559
[19] Antoniak C, Linder J and Farle M 2005 *Europhys. Lett.* **70** 250
[20] Bourlinos A B, Herrera R, Chalkias N, Jiang D D, Zhang Q, Archer L A and Giannelis E P 2005 *Adv. Mater.* **17** 234
[21] Atsarkin V A, Demidov V V and Vasneva G A 1995 *Phys. Rev.* B **52** 1290
[22] Dormann J L, D'Orazio F, Lucari F, Tronc E, Prené P, Jolivet J P, Fiorani D, Cherkaoui R and Noguès M 1996 *Phys. Rev.* B **53** 14291

[23] Martinez B, Obradors X, Balcells Ll, Rouanet A and Monty C 1998 *Phys. Rev. Lett.* **80** 181
[24] Raikher Yu L and Stepanov V I 1995 *J. Magn. Magn. Mater.* **149** 34
[25] Raikher Yu L and Stepanov V I 1995 *Phys. Rev.* B **51** 16428
[26] Abragam A 1961 *The Principles of Nuclear Magnetism* (Oxford: Clarendon)
[27] Birks J B 1950 *Proc. Phys. Soc.* B **63** 65
[28] Dzheparov F S 2006 private communication
[29] Kittel C 1996 *Introduction to Solid State Physics* (New York: Wiley)
[30] Dimitrov D A and Wysin G M 1997 *Phys. Rev.* B **54** 9237
[31] Garcia-Palacios J L and Lazaro F J 1997 *Phys. Rev.* B **55** 1006
[32] Roch A and Muller R N 1999 *J. Chem. Phys.* **110** 5403
[33] Noginova N, Bah R, Bitok D, Atsarkin V A and Demidov V V 2005 *J. Phys.: Condens. Matter* **17** 1259
[34] Seehra M S, Dutta P, Shim H and Manivannan A 2004 *Solid State Commun.* **129** 721
[35] Néel L 1954 *J. Phys. Radium* **15** 224
[36] Meiklejohn W H 1962 *J. Appl. Phys.* **33S** 1328
[37] Shilov V, Raikher Yu L, Bacri J C, Gazeau F and Perzynski R 1999 *Phys. Rev.* B **60** 11902
[38] Kodama R H and Berkowitz A E 1999 *Phys. Rev.* B **59** 6321
[39] Garanin D A and Kachkachi H 2003 *Phys. Rev. Lett.* **90** 065504
[40] De Biasi R S and Devezas T C 1978 *J. Appl. Phys.* **49** 2466
[41] Horng H E, Hong C Y, Yang H C, Jang I J, Yang S Y, Wu J M, Lee S L and Kuo F C 1999 *J. Magn. Magn. Mater.* **201** 215
[42] Noginova N and McClure J 2007 *Physica* B **393** 43